J. Phys. B: At. Mol. Opt. Phys. **30** (1997) 4791–4800. Printed in the UK PII: S0953-4075(97)85183-8

Photoelectron angular distribution measurements of C^- at visible wavelengths

D Calabrese†, A M Covington†, D L Carpenter†, J S Thompson†, T J Kvale‡ and R Collier§

† Department of Physics and Chemical Physics Program, University of Nevada, Reno, NV 89557-0058, USA

‡ Department of Physics and Astronomy, The University of Toledo, Toledo, OH 43606-3390, USA

§ Department of Physics, Western Nevada Community College, Carson City, NV 89703, USA

Received 19 June 1997, in final form 4 August 1997

Abstract. Photoelectron angular distributions for the laser photodetachment process $C^-(1s^2 2s^2 2p^3\ {}^4S) + h\nu \rightarrow C(1s^2 2s^2 2p^2\ {}^3P) + e^-$ have been measured at six wavelengths in the region 457.9–647.1 nm. An intense 10 keV C^- beam was produced in a caesium sputter-type ion source and mass-selected with a 90° bending magnet. The mass-selected ion beam was subsequently crossed at 90° with a linearly polarized, continuous photon beam. Angular distributions were obtained by measuring the laboratory-frame energy spectra of photodetached electrons as a function of the angle between the velocity vector of the ejected electrons and the polarization direction of the linearly polarized photon beam. The photoelectron angular distributions were used to determine asymmetry parameters. The present measurements are in excellent agreement with those of Hall and Siegel at 488.0 and 514.5 nm (1968 *J. Chem. Phys.* **48** 943), and good agreement with a calculation by Cooper and Zare (1968 *J. Chem. Phys.* **48** 942). The photodetachment asymmetry parameters for C^- are compared with a recent measurement of the photodetachment asymmetry parameters for Si^-.

1. Introduction

Photoelectron angular distributions have been valuable in uncovering salient features in single-photon, single-electron, ion–photon processes. The distributions are generally measured via the laser photoelectron spectroscopy (LPES) technique, where photoelectron yields are measured as a function of the angle θ between the polarization direction of a linearly polarized laser beam and the velocity vector of the photodetached electrons. It was shown by Bethe [1], for one-electron systems, and later by Cooper and Zare [2], for multi-electrons systems, that angular distributions of photoelectrons from photodetachment processes can be characterized by the form

$$\frac{d\sigma}{d\Omega} \propto [1 + \beta P_2(\cos\theta)] \tag{1}$$

where $P_2(\cos\theta)$ is the second-order Legendre polynomial. The above expression is valid for interactions between unpolarized targets and linearly polarized photons of energy $h\nu < 100$ eV. The asymmetry parameter β measures the anisotropy of the photoelectrons, and contains all the dynamic information of the ion–photon interaction. The restriction that the differential cross section is non-negative limits the asymmetry parameter to $-1 \leqslant \beta \leqslant 2$.

0953-4075/97/214791+10$19.50

For a process where $\beta = -1$, the photoelectron yield is maximized perpendicular to the polarization direction. When $\beta = 2$ the photoelectron yield is maximized parallel to the polarization direction. The asymmetry parameter is, in general, photon-energy dependent, and is affected by both the initial state of the negative ion and the anisotropic final-state interactions between the outgoing electron and the residual atomic core [3].

In the case of negative ion–photon interactions, the first experimental photoelectron angular distribution measurements were carried out for C^-, O^- and H^- by Hall and Siegel [4]. Since their pioneering work, there have been relatively few systematic angular distribution studies of photodetached electrons [5–8]. This is due to the small binding energy of the extra electron in the negative ion, which makes sample preparation difficult. As a result, there are few comparisons between theory and experiment. In this paper, a new set of measurements for the angular distributions of electrons photodetached from a beam of C^- is presented. The angular distributions were measured with a crossed ion–laser beam apparatus. This work is part of a continuing effort to systematically study photoelectron angular distributions in order to better understand the underlying principles governing photodetachment phenomena [5].

When visible wavelengths are used to photodetach a valence electron from the ground state of $C^-(1s^22s^22p^3\ ^4S)$, the only observed transition is $C^-(1s^22s^22p^3\ ^4S) + h\nu \rightarrow C(1s^22s^22p^2\ ^3P) + e^-$, where the kinetic energy of the photoelectron is the difference between the incoming photon energy and the electron affinity of C (1.2629 ± 0.0003 eV) [9]. Although photons with visible wavelengths at or below 490.70 nm are sufficiently energetic to excite the $1s^22s^22p^2\ ^1D$ state of neutral carbon, the spin angular momentum conservation rule prohibits the process [9]. To describe the photodetachment process, Ramsbottom *et al* [10] used an *ab initio* many-electron model to calculate the photodetachment cross section for C^-. Their results predicted a slowly increasing photodetachment cross section at visible wavelengths. Ramsbottom's *ab initio* calculation is in good agreement with an earlier single-electron model potential calculation by Robinson and Geltman [11]. The agreement between the independent-particle and many-electron calculations suggests that the contribution of correlation effects to the total photodetachment cross section is relatively small for the non-resonant collision process, as is expected for single-electron photodetachment processes involving light negative ions.

Within the independent-particle approximation, the photodetachment of $C^-(1s^22s^22p^3\ ^4S) + h\nu \rightarrow C(1s^22s^22p^2\ ^3P) + e^-$ produces outgoing s- and d-wave photoelectrons. The relative contribution of the competing channels depends upon the incident photon energy and the structure of the negative ion. Near threshold, the s-wave is expected to dominate, since the d-wave is suppressed by the centrifugal barrier [12]. Well beyond threshold, both photodetachment channels are active and will interfere.

In Hall and Siegel's [4] work, asymmetry parameters for the process $C^-(^4S) + h\nu \rightarrow C(^3P) + e^-$ were measured at photon wavelengths of 488.0 and 514.5 nm. Their measured asymmetry parameters were in good agreement with theoretical values obtained by Cooper and Zare [2]. In the Cooper–Zare [2] calculation, the energy dependence of the asymmetry parameter was obtained from an independent electron potential model [11], which contained adjustable parameters to give the correct binding energy of $C^-(^4S)$. Furthermore, the calculation did not include the final stage of the photodetachment phenomenon—the anisotropic interaction of the outgoing electron with the residual atom. The agreement between the experimental measurements and the calculation suggests that the term-dependent final-state interaction between the photoelectron and the short-range potential of the C atom is a small contribution to the asymmetry parameter. In this paper, we report asymmetry parameters for photodetaching C^- at four additional

wavelengths (six total) in order to explore the spectral dependence of the asymmetry parameter.

2. Experiment

Extensive details of the apparatus are discussed elsewhere [5, 13, 14]. However, a brief overview of the experimental apparatus is presented below. Figure 1 presents a schematic illustration of the apparatus. The apparatus was composed of a negative-ion accelerator and an interaction chamber where photoelectrons were produced, energy analysed and detected. The C^- ion beam was produced in a caesium-sputter negative ion source. The source operated by colliding Cs^+ ions with a negatively biased graphite target. Negative ions that are produced by the collision are accelerated to a potential of 10 kV, and are focused into a beam. The C^- ions were mass selected by passing the extracted beam through a 90° bending magnet. The mass resolution of the magnet ($\Delta m/m$) was approximately 0.5%, which was sufficient to fully resolve the isotopes of carbon. After traversing the exit aperture of the magnet, the mass-selected C^- ions were focused and steered into the interaction chamber. The base pressure of the interaction chamber was 1×10^{-6} Pa. Typical C^- beam intensities inside the interaction chamber were of the order of 1 μA.

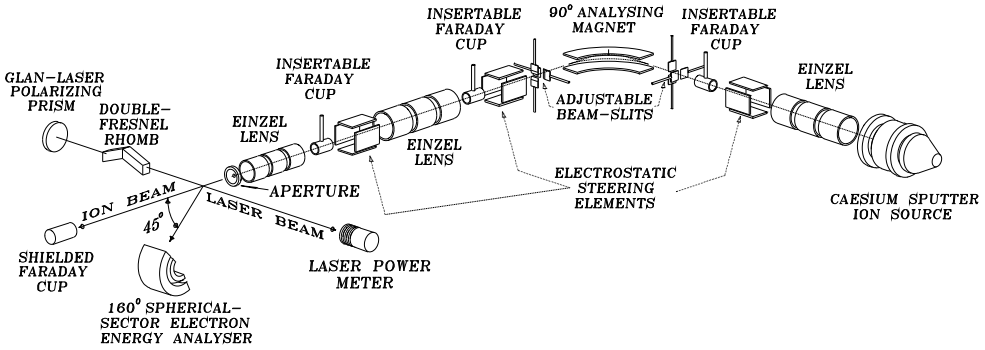

Figure 1. Schematic diagram of the experimental apparatus (see text for details).

Once inside the interaction chamber, the C^- ion beam intersected a linearly polarized, continuous (CW) photon beam at a crossing angle of 90°. The photon beams were produced by either a 25 W Ar^+ laser or a 1 W Kr^+ laser. A Glan–laser polarizing prism with an extinction ratio $\sim 10^{-5}$ was placed in the photon beam to ensure high polarization purity. Photoelectrons resulting from the ion–laser interaction were energy analysed by a 160° spherical-sector electron spectrometer. Since angular distributions depend upon the angle between the photoelectron collection direction and the direction of the polarization vector, the collection direction was fixed and the polarization direction was rotated with a double-Fresnel rhomb ($\lambda/2$ retarder). The photon beam was carefully positioned with respect to the C^- ion beam to maximize the overlap between the interacting beams, while minimizing laser beam 'walk' as the double-Fresnel rhomb was rotated. Sets of apertures near the interaction region ensured proper positioning of the crossed beams.

The electron spectrometer was operated at a constant pass energy of 20 eV. The energy resolution of the spectrometer ($\Delta E/E$) was approximately 0.4%, and was determined from the full width at half maximum of the measured photoelectron spectra. Electrons entering the spectrometer traversed a set of 0.50 mm diameter entrance apertures that were spaced

5.08 mm apart. Since the first entrance aperture was approximately 31.8 mm from the interaction region, the acceptance angle of the spectrometer was limited to less than $\pm 1^{\circ}$. The C(^{3}P) $J = 0 \rightarrow 1$ (2.03 meV) and $J = 0 \rightarrow 2$ (5.39 meV) fine-structure splittings are very small compared to the resolution of the electron spectrometer, and the resulting fine-structure transitions could not be observed [15]. To shield the ejected electrons from external magnetic fields, the electron spectrometer and interaction region were housed inside a μ-metal box. This reduced the field in the interaction region to less than 5 mG. Electrons transmitted through the spectrometer were detected with a Topac Inc. Scientific Instruments [16] channel electron multiplier operating in the pulse counting mode. The electron signal produced in the detector was subsequently amplified and discriminated to reduce background noise.

Output pulses from the discriminator were collected by a computer-controlled counter. The intensity of the laser and negative ion beams were monitored through two voltage-to-frequency converters that were connected to the analogue outputs of an electrometer and a laser power meter, respectively. The pulses from the voltage-to-frequency converters were subsequently collected by computer-controlled counters. The number of detected electrons

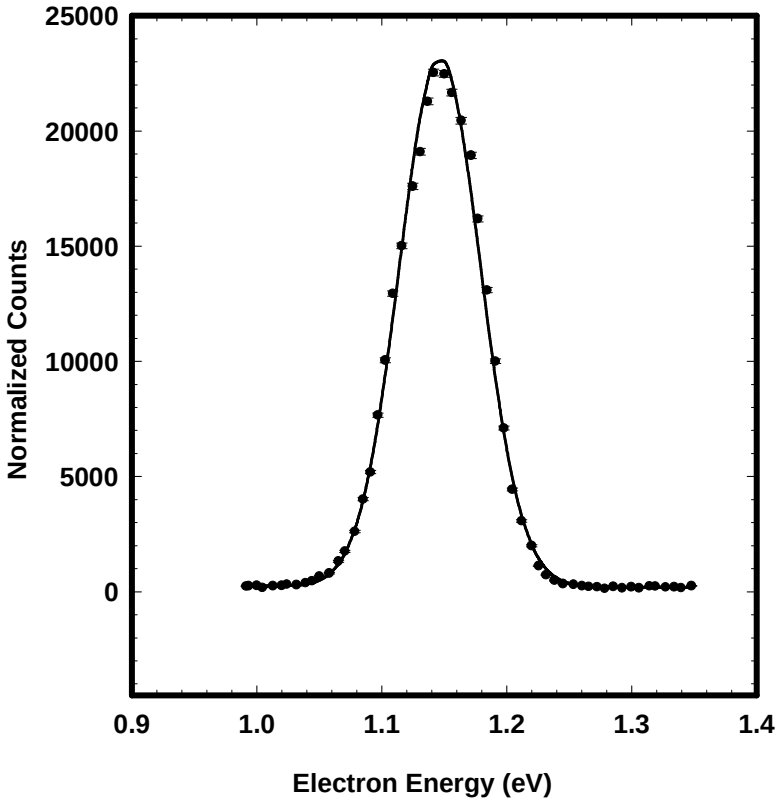

Figure 2. Photoelectron energy spectrum for the process $C^-(1s^2 2s^2 2p^3\ {}^4S) + h\nu \rightarrow C(1s^2 2s^2 2p^2\ {}^3P) + e^-$ plotted as a function of energy in the centre-of-mass frame. This energy- and angle-resolved spectrum was measured with the 514.5 nm line of a CW Ar^+ laser. The full curve represents a nonlinear least-squares fit of the experimental data (full circles) to a Gaussian curve weighted by the statistical uncertainty in each data point. Error bars represent the statistical uncertainty in each data point at one standard deviation. The fine-structure splittings of C(^{3}P) were too small to be resolved in this experiment.

was then normalized to the intensities of the negative ion and laser beams to account for variations in the beams with time. At each angle θ, photoelectron energy spectra were collected by stepping the acceleration voltage applied to the spectrometer. A PC-based data acquisition and control system processed incoming data for real-time display, and stored the data at the end of each energy scan. The data accumulation time for each energy scan was approximately 130 s. A typical energy- and angle-resolved photoelectron spectrum measured at a wavelength of 514.5 nm is shown in figure 2. Signal-to-noise ratios as high as 140:1 were observed during the experiment. C^- has an excited metastable ^{2}D state that is 1.2299 ± 0.001 eV above the ^{4}S ground state of C^-, therefore it was also possible to observe a $C^-(1s^22s^22p^3\ ^2D) \rightarrow C(1s^22s^22p^2\ ^1D)$ transition that is expected to partially overlap the observed $C^-(1s^22s^22p^3\ ^4S) \rightarrow C(1s^22s^22p^2\ ^3P)$ photoelectron peak. However, the measured spectra showed no evidence of the $C^-(1s^22s^22p^3\ ^2D) \rightarrow C(1s^22s^22p^2\ ^1D)$ transition, indicating that there were very few metastable $C^-(^2D)$ ions in the interaction region. Pegg *et al* [17] have recently reported photoelectron angular distributions of electrons photodetached from the ^{2}D excited state of C^-.

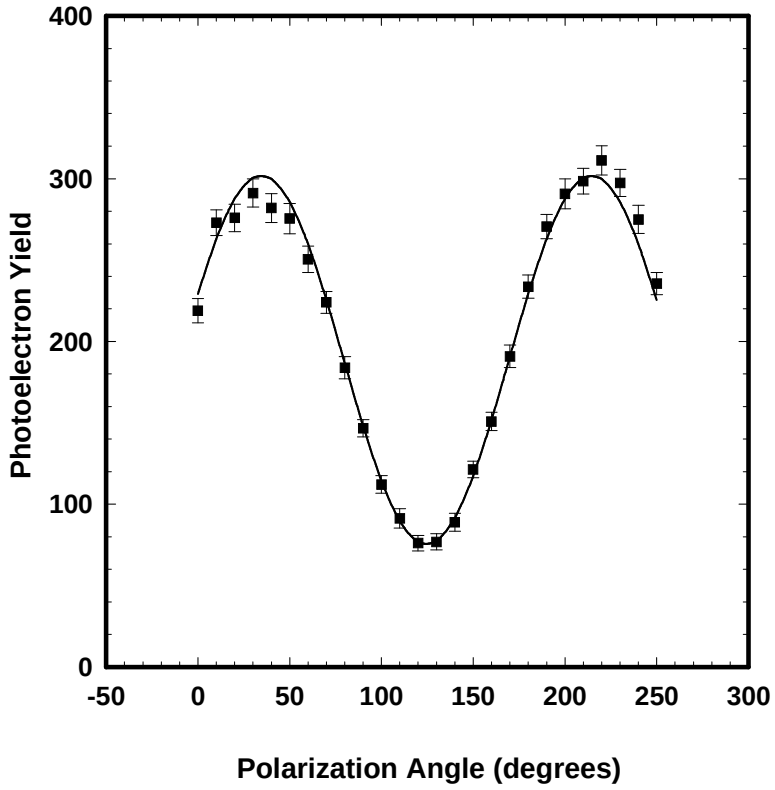

Figure 3. Photoelectron yields plotted as a function of the angle between the polarization direction of the photon beam and the photoelectron collection direction. Error bars associated with the photoelectron yields represent uncertainties of nonlinear curve fits to the Gaussian function, resulting from statistical uncertainties in the individual data points of each photoelectron spectrum. The extracted value of β for this particular angular distribution measurement at 457.9 nm is -0.67 ± 0.01. The error bar in β reflects the statistical uncertainty of the nonlinear curve fit described in the text, and is reported to one standard deviation.

After a set of energy spectra were collected, each photoelectron peak was fitted to a Gaussian function using a nonlinear least-squares routine that weighted each data point by its statistical uncertainty. The parameters that were extracted from the fit were then used to integrate the Gaussian to obtain the photoelectron yield and its uncertainty. Finally, the yields were plotted as a function of the dial setting of the polarization rotator, and fitted to equation (1) with weighting factors given by the uncertainties in the photoelectron yields.

An example of the photoelectron yields plotted as a function of the dial setting of the polarization rotator is shown in figure 3. It should be noted that the abscissa reflects a relative angle, not the angle θ. As a result, the asymmetry parameter was extracted from the data by fitting the yields to the expression $I(\theta) = a[1 + \beta P_2(\cos(\alpha - c))]$, where a, β and c are fitting parameters, and α is the dial setting of the polarization rotator. To obtain a physically reasonable value of β from the fit, the approximate dial setting in which the photoelectron collection direction was perpendicular to the direction of the polarization vector ($\theta = 90^\circ$) had to be determined. This was accomplished by inserting a polarization analyser into the laser beam after the double-Fresnel rhomb. The transmission axis of the analyser was set parallel to the electron collection direction, and the dial indication for which the photoelectron yield is minimized for a process where the value of the asymmetry parameter is near -1 was determined. Once the approximate dial setting corresponding to $\theta = 90^\circ$ was determined, then the fitting parameter β was restricted to a positive or negative value.

3. Results and discussion

A compilation of the measured asymmetry parameters is presented in table 1. The second column in table 1 gives the weighted averages of asymmetry parameters that were measured on several occasions. The quoted uncertainties result from an average weighting by the statistical uncertainties of the nonlinear curve fits. To determine systematic errors, the effects on the measured asymmetry parameters due to the time-dependent nature of the spatial overlap of the ion and laser beams, and the acceptance angle of the electron spectrometer had to be considered. In the latter case, the entrance aperture of the spectrometer was sufficiently small that solid-angle effects could be neglected. The variation of the spatial overlap between the two beams, on the other hand, was by far the largest source of uncertainty in the present experiment. An estimate of its effect on the measured asymmetry parameters was obtained by averaging the extracted values of β at each wavelength and calculating their standard deviation of the mean. The corresponding standard deviations of the means are presented in the third column of table 1. All uncertainties listed in table 1 are reported

Table 1. Summary of the measured asymmetry parameters for the process $C^-(^4S) + h\nu \rightarrow C(1s^2 2s^2 2p^2\ ^3P) + e^-$ as described in the text.

Wavelength (nm)	β, weighted average	Standard deviation of the mean
647.1	-0.89 ± 0.03	0.03
514.5	-0.79 ± 0.01	0.01
501.7	-0.783 ± 0.002	0.02
488.0	-0.718 ± 0.001	0.04
476.0	-0.68 ± 0.02	0.06
457.9	-0.67 ± 0.01	0.04

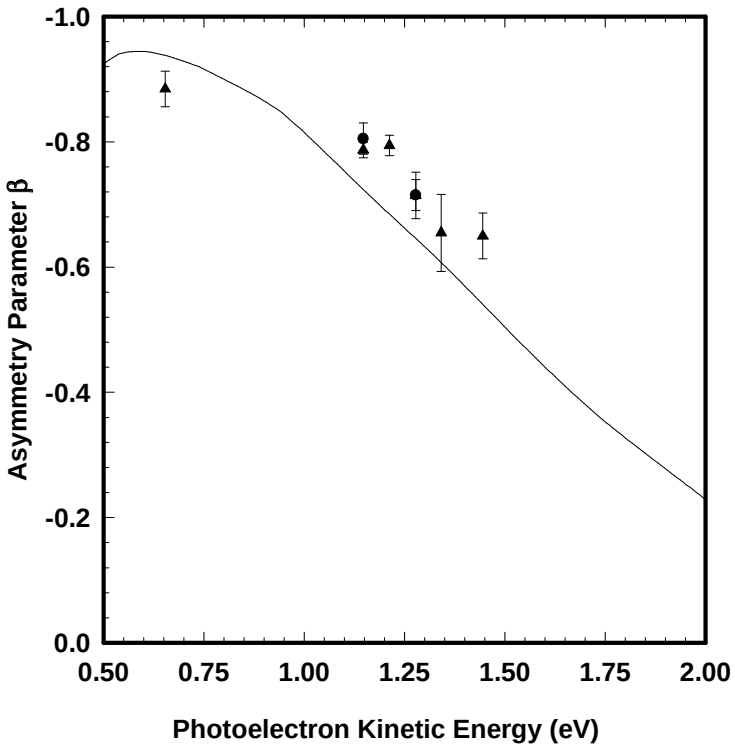

Figure 4. Measured asymmetry parameters (full triangles) plotted as a function of the photoelectron kinetic energy. The full curve represents the theoretically predicted spectral dependence of β for the process under investigation [2]. The full circles are the results of the experimental measurements of Hall and Siegel [4].

to one standard deviation of the weighted averages and means. The weighted averages of the asymmetry parameters, listed in the second column of table 1, and their corresponding standard deviations of the mean, listed in the third column of table 1, are plotted as a function of photoelectron kinetic energy in figure 4.

Figure 4 also shows the theoretical predictions of Cooper and Zare [2] and the experimental results of Hall and Siegel [4]. There is excellent agreement between the present work and that of Hall and Siegel [4]. The energy dependence of β measured in the present experiment is well predicted by Cooper–Zare theory [2]. The reliability of the Cooper–Zare calculation [2] can be better understood if it is compared to the angular momentum transfer theory that was initially developed by Fano and Dill [18–20] and reviewed by Manson and Starace [3].

Within the angular momentum transfer theory, the orbital angular momentum of the residual core couples with the orbital angular momentum of the continuum electron. The coupling yields several competing channels that interfere to produce angular distributions that could deviate significantly from the Cooper–Zare theory [2]. The angular momentum transferred by the photon to the ion is expressed as $\boldsymbol{j}_t = \boldsymbol{L}_c - \boldsymbol{L}_o$, where $\boldsymbol{L}_c$ and $\boldsymbol{L}_o$ are the orbital angular momenta of the residual atom and negative ion, respectively. Each value of $\boldsymbol{j}_t$ can either be parity favoured $\pi_o\pi_c = (-1)^{j_t}$, or unfavoured $\pi_o\pi_c = (-1)^{j_t+1}$. In the Cooper–Zare theory [2], the only allowed angular momentum transfer is parity favoured

and is given by $j_t = l_o$, where l_o is the orbital angular momentum of the electron that is photodetached from the negative ion. Under the Fano–Dill formalism [18–20], the effective asymmetry parameter is a weighted average of the form

$$\beta = \frac{\sum \sigma(j_t)\ \beta(j_t)}{\sum \sigma(j_t)} \tag{2}$$

where each cross section and asymmetry parameter associated with j_t is written in terms of photodetachment scattering amplitudes $S_{l_o \pm 1}(j_t)$.

In the present experiment, the interaction of the s- and d-wave photoelectrons with the residual $C(^3P)$ atom can only produce the parity-favoured angular momentum transfer $j_t = 1$, which gives rise to a single LS-coupled ^4P state. The effective asymmetry parameter for the photodetachment process is written as

$$\beta = \frac{3|S_d(1)|^2 - 3\sqrt{2}[S_d(1)S_s^*(1) + S_d^*(1)S_s(1)]}{3[|S_d(1)|^2 + |S_s(1)|^2]}. \tag{3}$$

Configuration interactions allow angular momentum transfer other than $j_t = 1$ that will produce term-dependent interactions of the continuum electron and the residual core. However, the good agreement between the measured asymmetry parameters and the Cooper–Zare calculation [2] suggests that the effect of final-state interactions on the photoelectron angular distributions is small in the present investigation. As a result, the asymmetry parameters for the process $C^-(1s^2 2s^2 2p^3\ ^4S) + h\nu \rightarrow C(1s^2 2s^2 2p^2\ ^3P) + e^-$ are well

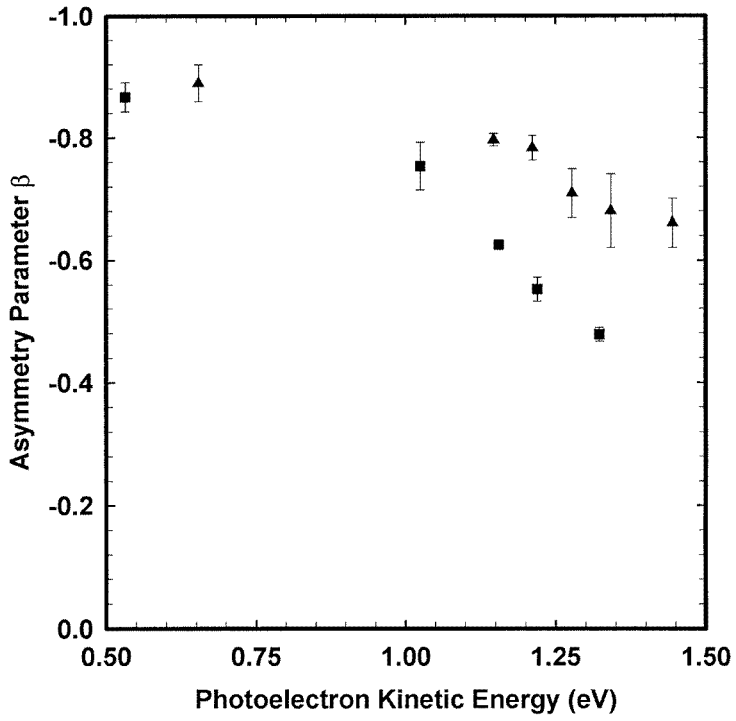

Figure 5. Comparison of the measured asymmetry parameters for C^- (triangles) and Si^- (squares) as a function of photoelectron kinetic energy. The Si^- measurements are from Covington *et al* [5].

described by the interference of the outgoing s- and d-wave electrons as in the Cooper–Zare model [2]. Furthermore, the reliability of the Cooper–Zare calculation [2] is primarily dependent upon the choice of the electric-dipole interaction between the $C^-(^4S)$ ion and the electromagnetic field.

The spectral dependence of the asymmetry parameter for photodetaching an electron from C^- can be compared with recent measurements [5] of the asymmetry parameters for photodetachment of Si^- at visible wavelengths. The electron affinity of silicon is 1.385 eV [21]. Photodetachment of Si^-, $Si^-([Ne]3s^23p^3\ ^4S) + h\nu \rightarrow Si([Ne]3s^23p^2\ ^3P) + e^-$, is analogous to photodetachment of a 2p electron from $C^-(^4S)$. Photodetachment of ground-state C^- and Si^- both result in the detachment of a p-electron at visible photon wavelengths in an independent electron model. Both photodetachment processes also share the same *LS* coupled initial and final states. In addition, the form of the asymmetry parameter, as described by angular momentum transfer theory, is identical for single-photon detachment of $C^-(^4S)$ and $Si^-(^4S)$. Figure 5 shows a comparison of asymmetry parameters for photodetaching $C^-(^4S)$ and $Si^-(^4S)$ as a function of photoelectron kinetic energy in eV. The spectral dependences and numerical values of the asymmetry parameters for photodetachment from both ions at visible wavelengths are similar. This leads to the conclusion that the same physical processes should dominate a description of the photodetachment process for these two ions.

4. Conclusion

Photoelectron angular distributions for the process $C^-(1s^22s^22p^3\ ^4S) + h\nu \rightarrow C(1s^22s^22p^2\ ^3P) + e^-$ have been measured with a crossed ion–laser beam apparatus. The measurements were carried out at six wavelengths in the region 457.9–647.1 nm. The angular distributions were used to extract asymmetry parameters, which describe the anisotropy of the outgoing electrons. The results were compared to the theoretical calculations of Cooper and Zare [2] and the experimental findings of Hall and Siegel [4]. The agreement of the present measurements with both the previous measurements and the Cooper–Zare theory [2] suggests that the effects of final-state interactions on the photoelectron angular distributions are small compared to the outgoing s- and d-wave interferences in influencing the spectral dependence of the asymmetry parameters for the process $C^-(1s^22s^22p^3\ ^4S) + h\nu \rightarrow C(1s^22s^22p^2\ ^3P) + e^-$. A comparison of the asymmetry parameters for the photodetachment of C^- and Si^- implies that the underlying principles governing their angular distributions at visible wavelengths are similar in nature.

Acknowledgments

Financial support from NSF is gratefully acknowledged under cooperative agreement OSR-9353227. TJK gratefully acknowledges support from a grant from the Division of Chemical Sciences, Office of Basic Energy Sciences, Office of Energy Research, US Department of Energy. RC and JST gratefully acknowledge support from a grant from the Nevada NSF-EPSCoR TREC programme.

References

[1] Bethe H A 1933 *Handbuch der Physik* vol 24 (Berlin: Springer) p 483
[2] Cooper J and Zare R 1968 *J. Chem. Phys.* **48** 942
[3] Manson S T and Starace A F 1982 *Rev. Mod. Phys.* **54** 389

[4] Hall J L and Siegel M W 1968 *J. Chem. Phys.* **48** 943
[5] Covington A M, Calabrese D, Williams W W, Thompson J S and Kvale T J *Phys. Rev.* A to be published
[6] Hanstorp D, Bengtsson C and Larson D J 1989 *Phys. Rev.* A **40** 670
[7] Thompson J S, Pegg D J, Compton R N and Alton G D 1990 *J. Phys. B: At. Mol. Opt. Phys.* **23** L15
[8] Liu Y, Pegg D J, Thompson J S, Dellwo J and Alton G D 1991 *J. Phys. B: At. Mol. Opt. Phys.* **24** L1
[9] Feldmann D 1977 *Chem. Phys. Lett.* **47** 338
[10] Ramsbottom C A, Bell K L and Berrington K A 1993 *J. Phys. B: At. Mol. Opt. Phys.* **26** 4399
[11] Robinson E J and Geltman S 1967 *Phys. Rev.* **153** 4
[12] Wigner E P 1948 *Phys. Rev.* A **73** 1002
[13] Calabrese D, Covington A M and Thompson J S 1996 *J. Chem. Phys.* **105** 2936
[14] Alton G D 1986 *Nucl. Instrum. Methods* A **244** 133
Alton G D 1993 *Nucl. Instrum. Methods* B **73** 221
[15] Moore C 1949 *Atomic Energy Levels (Natl Bur. Standards (US) Circ.* no 467) (Washington, DC: US Govt Printing Office)
[16] Topac Inc.-Scientific Instruments, Hingham, MA, 02043
[17] Pegg D J, Yang C Y, Dellwo J and Alton G D 1993 *J. Phys. B: At. Mol. Opt. Phys.* **26** L789
[18] Dill D and Fano U 1972 *Phys. Rev. Lett.* **29** 1203
[19] Fano U and Dill D 1972 *Phys. Rev.* A **6** 185
[20] Dill D, Starace A F and Manson S T 1975 *Phys. Rev.* A **11** 1596
[21] Kasdan A, Herbst E and Lineberger W C 1975 *J. Chem. Phys.* **62** 541